



On the stress field redistribution of tool–chip interface for micro-groove textured tools

Junsheng Zhang^{1,2} · Yongsen Shang¹ · Haidong Yang¹ · Huohong Tang¹ · Shunhua Chen¹

Received: 8 October 2022 / Accepted: 15 April 2023 / Published online: 24 April 2023
© The Author(s), under exclusive licence to Springer-Verlag London Ltd., part of Springer Nature 2023

Abstract

The stress field redistribution at the tool–chip interface of micro-textured tools was examined. The effect of stress field redistribution on the cutting performance was also investigated, including cutting forces, friction characteristics, and chip morphology. The findings have shown that the main cutting forces were reduced by 18% through the decrease of average shear strength and tool–chip contact area. The equivalent average friction coefficient u_a decreased from 0.66 to 0.64 with the groove texture width increasing from 80 to 140 μm . The chip deformation coefficient also decreased from 3.4 to 2.77 with the increase of groove texture width, which was mainly attributed to the improvement of friction characteristics at the tool–chip interface. In order to characterize the stress field redistribution at the tool–chip interface, an improved theoretical model of stress field redistribution for micro-textured tool was proposed based on Zorev’s assumption. The stress field was assumed as zero in the groove texture zone and had a maximum local stress because of the appearance of derivative cutting. The proposed model was validated by the calculations of normal and friction forces. Combined with the theoretical calculations and experimental findings, the results have shown that with the increase of groove texture width, the decrease of normal and shear stress in the groove texture zone was enlarged. And the increase of normal and shear stress, caused by derivative cutting, was reduced. Then, under the combined effect of groove texture and derivative cutting, the friction characteristics at the tool–chip interface can also be improved. The present findings give more insight in to the stress field redistribution of micro-groove textured tools and the underlying friction mechanisms at tool–chip interface.

Keywords Stress field redistribution · Micro-texture · Cutting force · Friction characteristics · Derivative cutting

1 Introduction

Surface micro-texture was firstly proposed in the field of tribology and then employed extensively in the field of material processing. In general, micro-textured tools are mainly used to process difficult-machining-materials, such as stainless steel, titanium alloy [1, 2], superalloy and high strength steel [3, 4]. It has been proved that micro-textures can effectively improve the friction characteristics of tool–chip interface [5–7]. The cutting performance and tool life can then be

improved [8–10]. Micro-textured tools show great application potential for materials processing and attract a great deal of research attentions during the past decades [11].

The cutting performance and corresponding mechanisms of textured tools have been comprehensively studied in terms of cutting force, temperature, tool wear, surface roughness, and chip morphology [12, 13]. For example, Chen et al. [14] investigated the cutting performance of carbon steel with micro-grooved textures. It showed that the thrust force can be reduced up to 14.68%, compared with untextured inserts, which was mainly due to the decrease of friction at the tool–chip interface. Orra et al. [15] studied the combined effect of micro-textures and magneto-rheological damper on the cutting performance and revealed maximum percentage decrease in cutting force of about 30.07% and tool wear of about 73.21%. Besides, the tool–chip contact length variation of micro-textured tools during machining Ti-6Al-4V was also analyzed. And the effects of texture parameters on cutting forces and chip morphology like chip compression

✉ Haidong Yang
yanghaidonghfut@126.com

✉ Shunhua Chen
shchen@hfut.edu.cn

¹ School of Mechanical Engineering, Hefei University of Technology, Hefei 230009, China

² Key Laboratory of Electric Drive and Control of Anhui Province, Wuhu 241000, China

ratio were also examined [16]. Micro-grooves with different directions were designed on the tool rake face to machine Ti-6Al-4V alloy [17]. Compared with untextured insert, the tool wear behavior at the tool–chip interface and surface roughness of the machined surface can be further improved simultaneously. For example, Kishawy et al. [18] investigated the influence of micro-textures on the behavior of derivative cutting and pointed out that the position and width of micro-grooves were the most influential parameters for cutting forces, temperature, and tool wear. Zou et al. [19] studied the cutting performance and chip morphology of machining Inconel 718 with micro-groove structured tools. The results revealed the wear suppressing and chip breaking mechanism of micro-groove structured tools.

With the development of surface texturing technology, textures with different scales, types, and parameters have been proposed in previous studies [20–22]. For example, volcano-like textures were proposed for the machining of Ti6Al4V, and the cutting performance in terms of cutting force, cutting temperature, chip morphology, and tool wear was studied based on experimental and simulative methods [23]. Avadhoot et al. [24] studied the wear behavior and tool life of different types of textured tools. It was found that the tool life of micro-channel textured tools was increased by 60% when compared with that of micro-dimple textured tools at lower-speed machining. Different from conventional textures on the rake face of inserts, Takahashi et al. [25] proposed new textures on the insert flank face to further suppress the chatter vibration and flank adhesion. Wang et al. [26] have also examined the cutting performance of oxygen-free copper using four types of micro-textures, including straight grooves, concentric circulars, ring sequences, and mesh textures. Besides, multiscale textures combined with microscale textures and nanoscale textures [27] have also been proposed to improve the cutting performance of AISI H13 steel, respectively. Hybrid textures with grooves in sticking zone and dimples in sliding zone can also reduce the severe friction state at the tool–chip interface, improving the cutting performance [28].

Due to the combined effect of textures and lubrication conditions, interface friction characteristics can also be improved by surface textures. The modification of cutting fluid and lubrication state is another important issue for textured tools [29]. Gajrani et al. [30] studied the effect of nanogreen cutting fluid (NGCF) lubrication on the micro-textured tool–chip interface friction behavior, surface roughness, and chip morphology. The effect of nanofluid lubrication on the tribological properties of micro-textured TiC-based ceramic was then conducted [31]. Compared with traditional water-based cutting fluid, the 0.5 vol.% Fe₃O₄ nanofluid lubrication reduced the friction coefficient of about 45%. Additionally, Zhang et al. [32] revealed the coupling effect of magnetic nanofluids and micro-textures under magnetic field during

the machining of 45 steel. With the turning of 316 L stainless steel, the combined effect of micro-textures, magnetic field intensity, and Fe₃O₄ nanofluid lubrication on cutting performance also was studied [33].

Many studies have been conducted to uncover the cutting performance and mechanism of textured tools. It has been proved that appropriate surface micro-textures can improve the tool–chip interface friction characteristics with lubrication. The stress field distribution at the tool–chip interface is closely related to the friction characteristics. The improvement of friction characteristics is accompanied by the redistribution of stress field. However, although it is necessary to study the stress field redistribution of textured tools to reveal the friction mechanisms of tool–chip interface, the investigations on the stress field redistribution of textured tools have rarely been reported. In this work, the stress field redistribution on the rake face of YT15 micro-grooved tools will be analyzed by experimental investigations and theoretical calculations. The effect of stress field redistribution on the cutting force, friction characteristics, and chip morphology will also be examined and discussed.

2 Experiments

2.1 Cutting conditions

AISI 1045 steel bar, with a diameter of 70 mm and a length of 400 mm, was used as workpiece material. The cutting tools are commercial WC-TiC/Co cemented carbide inserts (YT15). The compositions, physical performance, and working geometrical parameters of the YT15 inserts are presented in Table 1. Turning was conducted on a CA6140 lathe, supplied with water-miscible cutting fluid (JR3A, 2.5%). During machining, the cutting force was measured by the high-resolution and high-reliability three-dimensional dynamometer (Kistler 9257B). A frequency converter (3G3RV-A4075-ZV) was equipped on the CA6140 lathe to keep the cutting speed

Table 1 Compositions, physical properties, and geometrical parameters of YT15 inserts

Compositions (wt%)		Working geometrical parameters	
TiC	15	Working cutting edge angle K_{re}	42°
WC	79	Rake angle γ_{oe}	-8°
Co	6	Clearance angle α_{oe}	18°
Physical performance		Inclination angle λ_{se}	0°
Density (g/cm ³)	11.5	Corner radius γ_e	0.5 mm
Hardness (HRA)	91		
Flexural strength (MPa)	1180		

as constant when the workpiece diameter decreased. The machining device is shown in Fig. 1.

2.2 Texturing

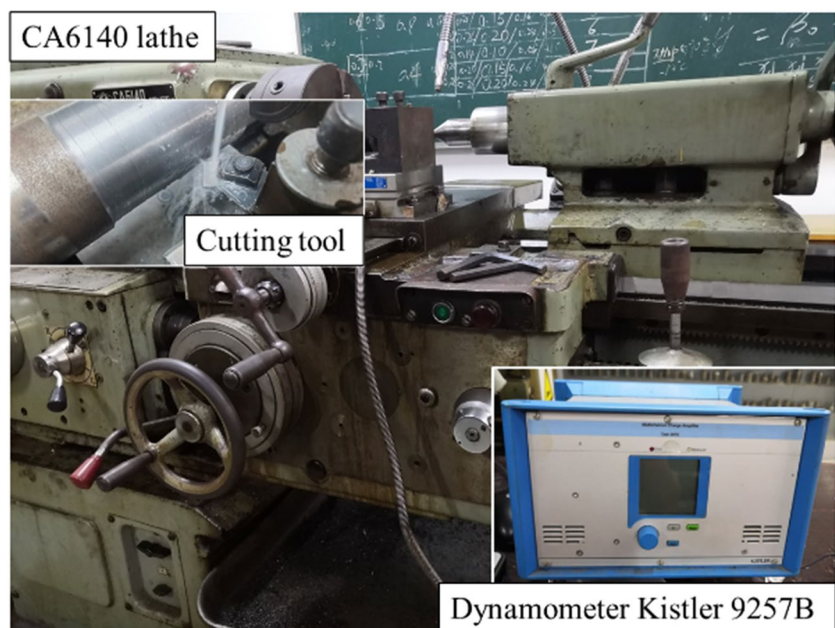
In order to study the stress field redistribution at the tool–chip interface, micro-grooved tools are used, as compared with untextured tools. Different from micro-pits and other textures, micro-grooves can effectively control the tool–chip contact length along the chip flow direction, which will be helpful to analyze the stress field distribution and friction characteristics at the tool–chip interface. Numerous studies have shown that the micro-groove textures can effectively improve the friction characteristics at the tool–chip interface with lubrication. The cutting performance can also be improved by appropriate groove texture parameters, including width, pitch, depth, and distance from the main cutting edge. The texture parameters in this study are selected based on previous results [34]. The fiber laser engraving machine YLP-F10 was used to fabricate micro-groove textures on the YT15 tools rake face. The plus frequency and wavelength of the fiber laser engraving machine are 20–100 kHz and 1.06 μm , respectively. After texturing, burrs on the edges of the groove textures were eliminated by polishing. The textured tools were then ultrasonic cleaned in anhydrous ethanol solution to further remove the residuals in the groove textures. Finally, the texture parameters were checked using a 3D laser measurement microscope VK-X250. In order to accurately control the actual tool–chip contact length, single groove texture with different widths was designed on the

tool rake face. The groove width G_w increased from 80 to 140 μm . And the groove depth G_d was about 20 μm , and the distance from the main cutting edge G_s was about 260 μm . Figure 2 shows the textured tools with different texture parameters after machining. The texture parameters and fiber laser engraving machine processing parameters are given in Table 2.

2.3 Turning

The turning process was conducted on the CA6140 lathe, as shown in Fig. 1. Single groove textured tools, with different widths (noted as S1, S2, S3, and S4, respectively), and untextured tool (S0), were prepared, as presented in Table 2. In order to achieve a relatively stable cutting process, medium cutting speed, low feed rate, and cutting depth were used based on previous studies [34]. The cutting speed v , cutting depth a_p , and feed rate f were 135 m/min, 0.2 mm, and 0.09 mm/r, respectively. During machining, the cutting forces were measured by the three-dimensional dynamometer Kistler 9257B. For each condition, the machining time was about 10 seconds, and the machining process was repeated three times to ensure the reliability of cutting forces. Zero drifts of the dynamometer were eliminated, and average cutting force values were calculated and recorded. Since the chip deformation can be influenced by the tool–chip interface friction behavior, the chips were also collected during machining, and the chip morphology was analyzed with scanning electron microscopy (SEM).

Fig. 1 CA6140 lathe and the three-dimensional dynamometer Kistler 9257B



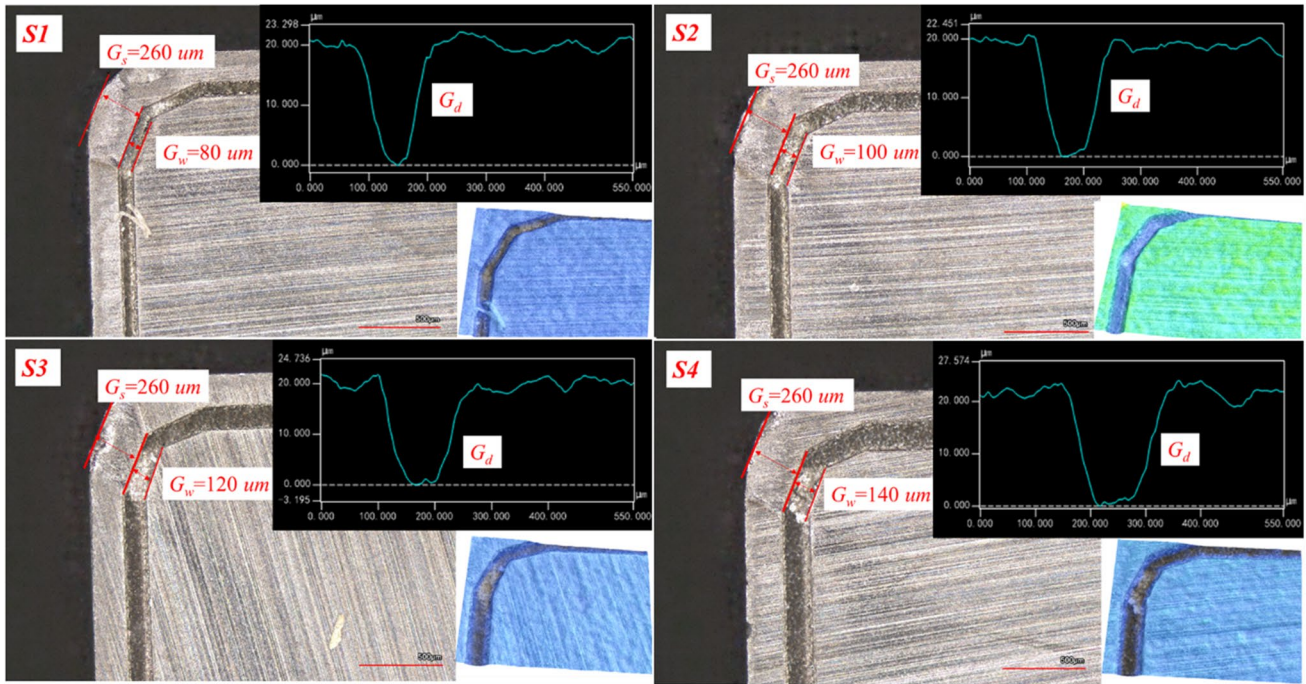


Fig. 2 Texture parameters checked by the 3D laser measurement microscope VK-X250

3 Cutting performance

3.1 Cutting forces

The axial force F_x , radial force F_y , and main cutting force F_z were measured during the machining of 45 steel with lubrication. Typical cutting forces of textured tools (S1, S2, S3, and S4) and untextured tool S0 with the same cutting parameters ($v = 135$ m/min, $a_p = 0.2$ mm, and $f = 0.09$ mm/r) were presented in Fig. 3. The cutting forces were analyzed, as shown in Fig. 4. It showed that the cutting forces of textured tools were generally much lower than that of untextured tools. On the other hand, the cutting forces decreased gradually with the increase of groove width. The results indicated that the micro-groove textures with lubrication on the tool rake face can reduce the cutting forces.

The cutting forces were mainly influenced by the shear stress τ_s and normal stress σ_s at the tool–chip interface. The introduction of groove texture can change the distribution of shear stress and normal stress. Here, the friction force, F_f , of the tool–chip interface can be expressed as

$$F_f = A_r \tau_c \tag{1}$$

where A_r is the tool–chip contact area and τ_c is the average shear strength. The average shear strength is determined by the percentage of metal adhesion area shear strength and the lubrication layer shear strength. Micro-groove textures on the tool rake face can enlarge the percentage of lubrication layer, which will reduce the average shear strength of the tool–chip interface. The friction force F_f will then be reduced. Besides, the introduction of groove texture reduced

Table 2 Texture parameters and fiber laser engraving machine processing parameters

Texture parameters			Laser processing parameters			
No.	Width	Depth	Distance	Scanning speed	Texturing times	Power
S0	-	-	-	-	-	-
S1	80 μm	20 μm	260 μm	280 mm/s	4	3.4 W
S2	100 μm					
S3	120 μm					
S4	140 μm					

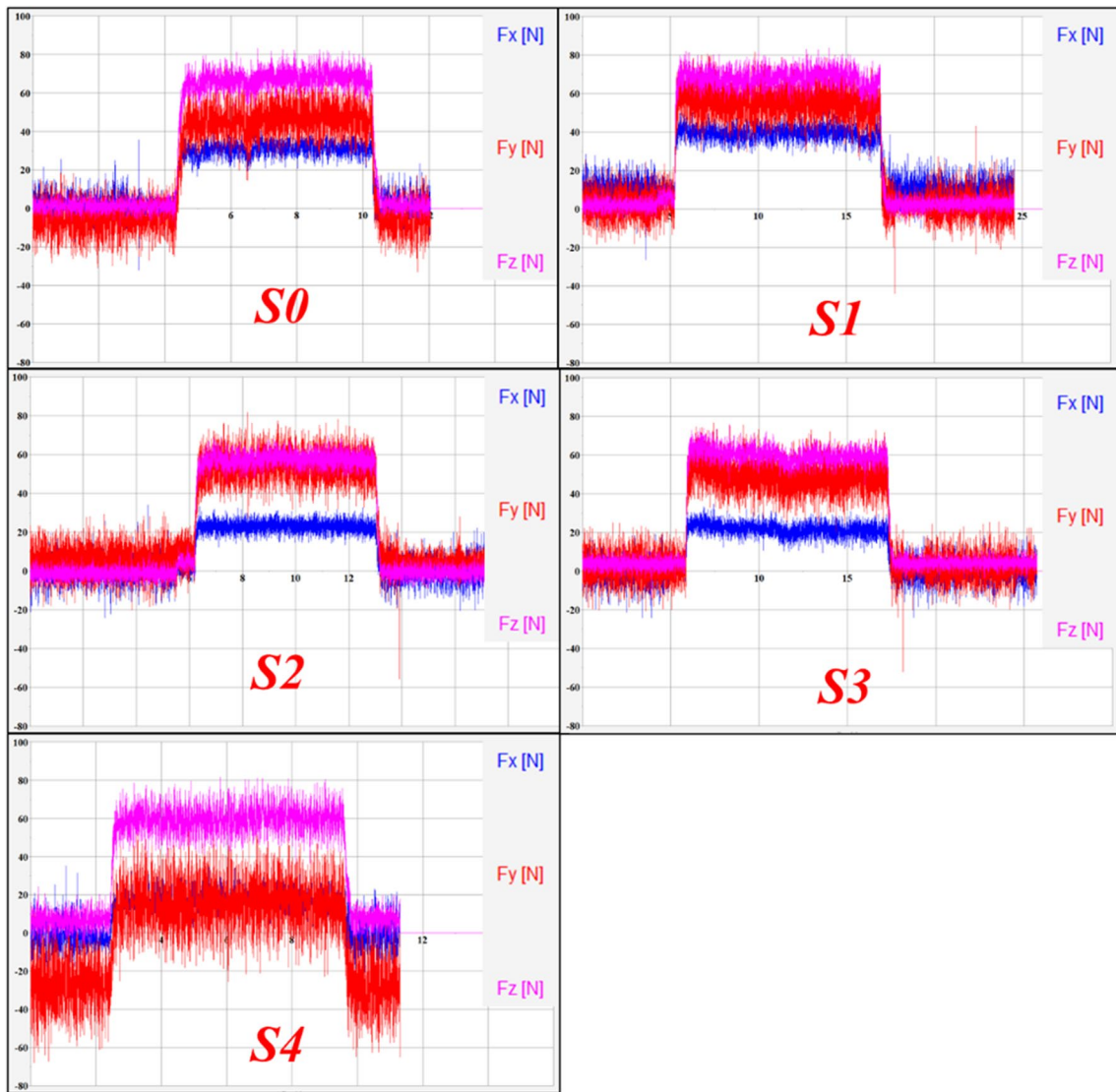


Fig. 3 The cutting forces measured by the dynamometer

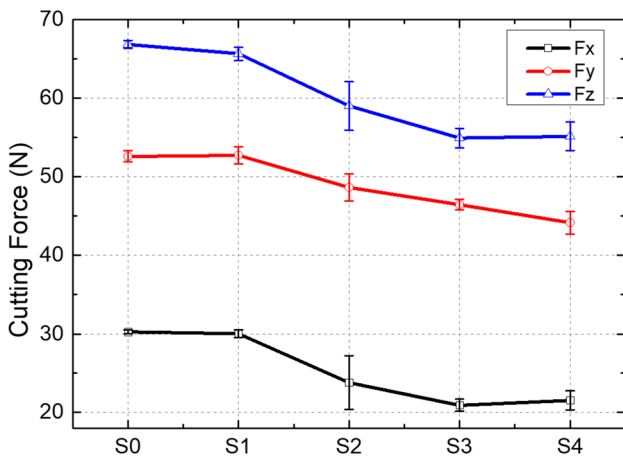


Fig. 4 Cutting forces of different cutting tools

the tool–chip contact area, and the normal force F_N was also reduced. Therefore, the cutting forces of textured tools were much lower than that of untextured tools as shown in Fig. 4.

More importantly, the cutting forces of textured tools S1 almost the same as untextured tools S0. Here, the width of single groove texture was $80\ \mu\text{m}$. It seemed that the effect of micro-texture on cutting force was missing here. In fact, the derivative cutting can also influence the cutting forces [18]. During machining, the edge of groove texture cut the bottom of the chip. The edge of the groove texture then became a new cutting edge. Many small chips came up in the groove texture because of derivative cutting, as shown in Fig. 5. The derivative cutting presented a secondary cutting of chips, which increased the local stress near the edge of groove texture. Therefore, the stress field distribution was changed, and the cutting force was also enlarged. In conclusion, the

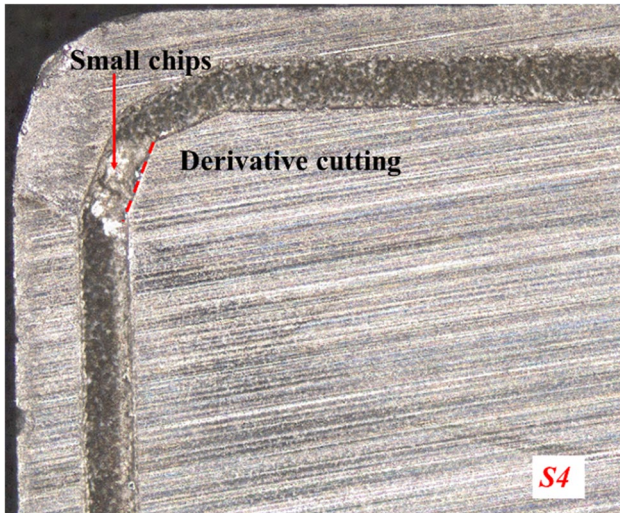


Fig. 5 Derivative cutting on the edge of groove texture

groove textures can reduce the cutting forces by reducing the average shear strength and tool–chip contact area. On the other hand, it will also enlarge the cutting forces with the appearance of derivative cutting. When their effects on cutting forces are about the same, the cutting forces of textured tools will be almost the same as untextured tools, such as S1. With the increase of groove texture width, the reduction of cutting forces can be further amplified. The cutting force of textured tools will be much lower than that of untextured tool, such as S2, S3, and S4 in this work.

3.2 Friction characteristics

In addition to the cutting force, the friction characteristics of the tool–chip interface was also affected by the micro-textures. Generally, the friction characteristics of the tool–chip interface can be expressed by the average friction coefficient u . Theoretical modelling of orthogonal cutting process was usually conducted to analyze the cutting forces. The average friction coefficient u can be calculated by radial force F_y , main cutting force F_z , and tool rake angle γ_{oe} :

$$u = \tan [\arctan (F_y/F_z) + \gamma_{oe}] \tag{2}$$

According to previous studies [35], the actual three-dimensional cutting process can be approximated to orthogonal cutting. The axial force F_x was then neglected during the analysis of friction characteristics. However, differing from orthogonal cutting, the actual turning process was usually three-dimensional. In order to present the average friction coefficient more accurately, the axial force F_x was also considered in this work. An improved calculation method of average friction coefficient was then conducted with considering axial force F_x . Here, the cutting edge, participated in cutting, can be approximated to a straight line, and the actual three-dimensional cutting process was simplified, as shown in Fig. 6.

The equivalent average friction coefficient u_a can then be expressed by the equations:

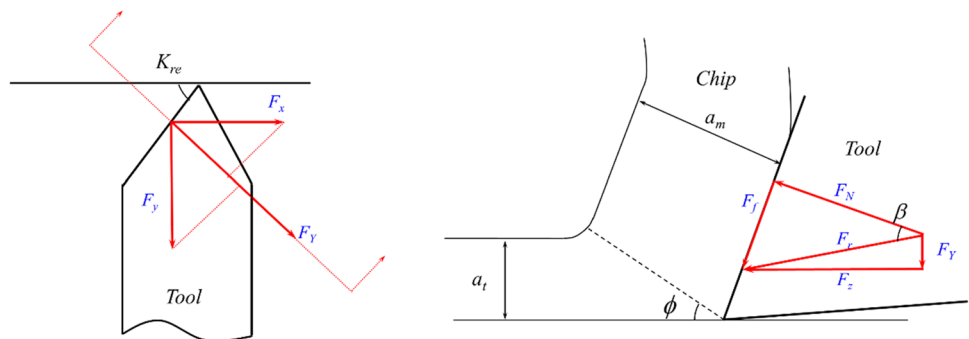
$$u_a = \tan [\arctan (F_Y/F_z) + \gamma_{oe}] \tag{3}$$

$$F_Y = F_x \cdot \sin K_{re} + F_y \cdot \cos K_{re}. \tag{4}$$

where the equivalent radial force F_Y was the comprehensive result of axial force F_x and radial force F_y . Figures 7 and 8 showed the results of equivalent radial forces F_Y and equivalent average friction coefficient u_a , respectively.

The results showed that the equivalent radial force F_Y and equivalent average friction coefficient u_a decreased gradually with the increase of groove texture width. In particular, the equivalent average friction coefficient of S1 was larger than that of untextured insert S0. It was mainly caused by the derivative cutting, which presented a secondary cutting of chips. Then, the local stress near the edge of groove texture was increased as mentioned above. The friction characteristics between the tool–chip interface was worsened, and equivalent average friction coefficient was also enlarged. Except for that, the variation trends of equivalent radial forces and average friction coefficient were basically consistent with that of cutting forces. Based on the theoretical model of orthogonal cutting, the resultant force F_r can be calculated as [35]:

Fig. 6 The new calculation method of average friction coefficient with considering of axial force



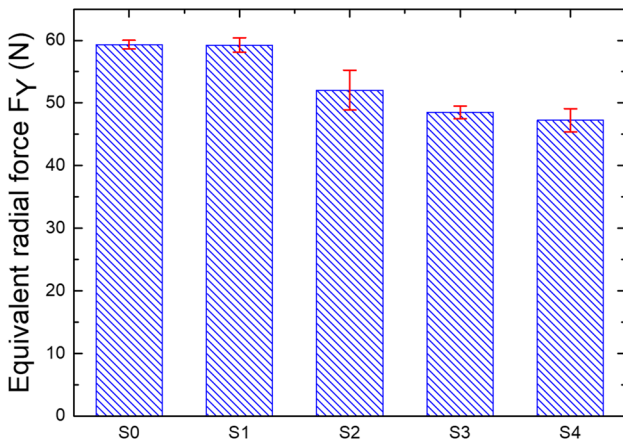


Fig. 7 Equivalent radial force of cutting tools

$$F_r = a_w l_f \tau_c / \sin \beta \tag{5}$$

$$l_f = f \cdot \sin K_{re} \cdot \frac{\eta + 2}{2} \cdot \frac{\sin(\phi + \beta - \gamma_{oe})}{\sin \phi \cos \beta} \tag{6}$$

where l_f is the theoretical tool–chip contact length, a_w is the cutting width, η is the normal stress field distribution index, ϕ is the shear angle, and β the friction angle. The resultant force, F_r , can also be calculated by the workpiece material shear strength τ_w :

$$F_r = \frac{a_w f \sin K_{re} \tau_w}{\sin \phi \cos(\phi + \beta - \gamma_{oe})} \tag{7}$$

Combining equations (5), (6), and (7), the friction angle β can be obtained. Finally, the relationship between equivalent average friction coefficient u_a and average shear strength of the tool–chip interface τ_c can be presented as

$$u_a = \tan \beta \tag{8}$$

$$\beta = \frac{\arcsin \left[\frac{\tau_c(\eta+2) \sin 2(\phi+\beta-\gamma_{oe})}{2\tau_w} \right]}{2} \tag{9}$$

As mentioned above, the average shear strength τ_c will be reduced with the introduction of micro-texture. Therefore, the equivalent average friction coefficient u_a will decrease gradually with the increase of groove texture width, as shown in Fig. 8.

3.3 Chip morphology

As mentioned before, the groove texture can affect the friction characteristics of tool–chip interface, which will also affect the chip deformation. In order to study the effect of groove texture on the chip shear deformation, SEM was conducted to analyze the chip morphology. Figure 9 showed the SEM micrographs of the chip free surface, back surface, and side surface for textured and untextured tools. The results showed that the chips were mainly characterized with plastic deformation. And serrated chips were formed by extrusion deformation. The chip morphology was presented as shown in Fig. 9. The chip thickness a_m was measured to analyze the chip deformation coefficient ξ . The cutting thickness a_t can be calculated by the following equation:

$$a_t = f \cdot \sin K_{re} \tag{10}$$

And the chip deformation coefficient ξ can be expressed as

$$\xi = \frac{a_m}{a_t} \tag{11}$$

Figure 10 showed the chip deformation coefficient for textured and untextured tools. It indicated that the chip deformation coefficient decreased gradually from 3.4 to 2.77 with the increase of groove texture width. Then, the shear angle of workpiece material can be presented as

$$\tan \phi = \frac{\cos \gamma_{oe}}{\xi - \sin \gamma_{oe}} \tag{12}$$

Based on the measured chip thickness, the shear angles can be calculated, and the results are shown in Fig. 11. The shear angle increased from 15.6 to 18.8° with the increase of groove texture width. The theoretical model of shear angle can also be expressed as

$$\phi = \pi/4 + \gamma_{oe}/2 - \beta/2 \tag{13}$$

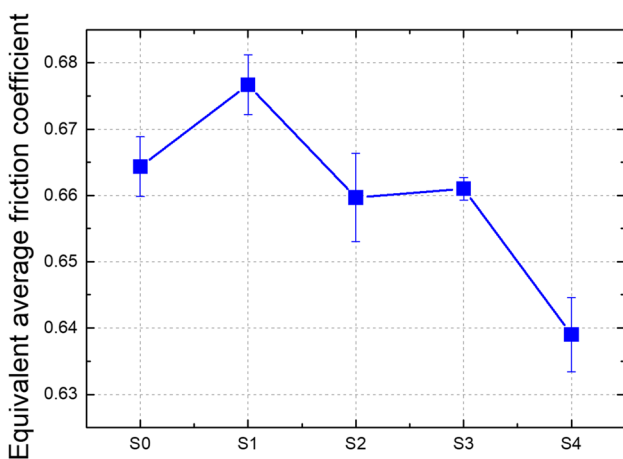
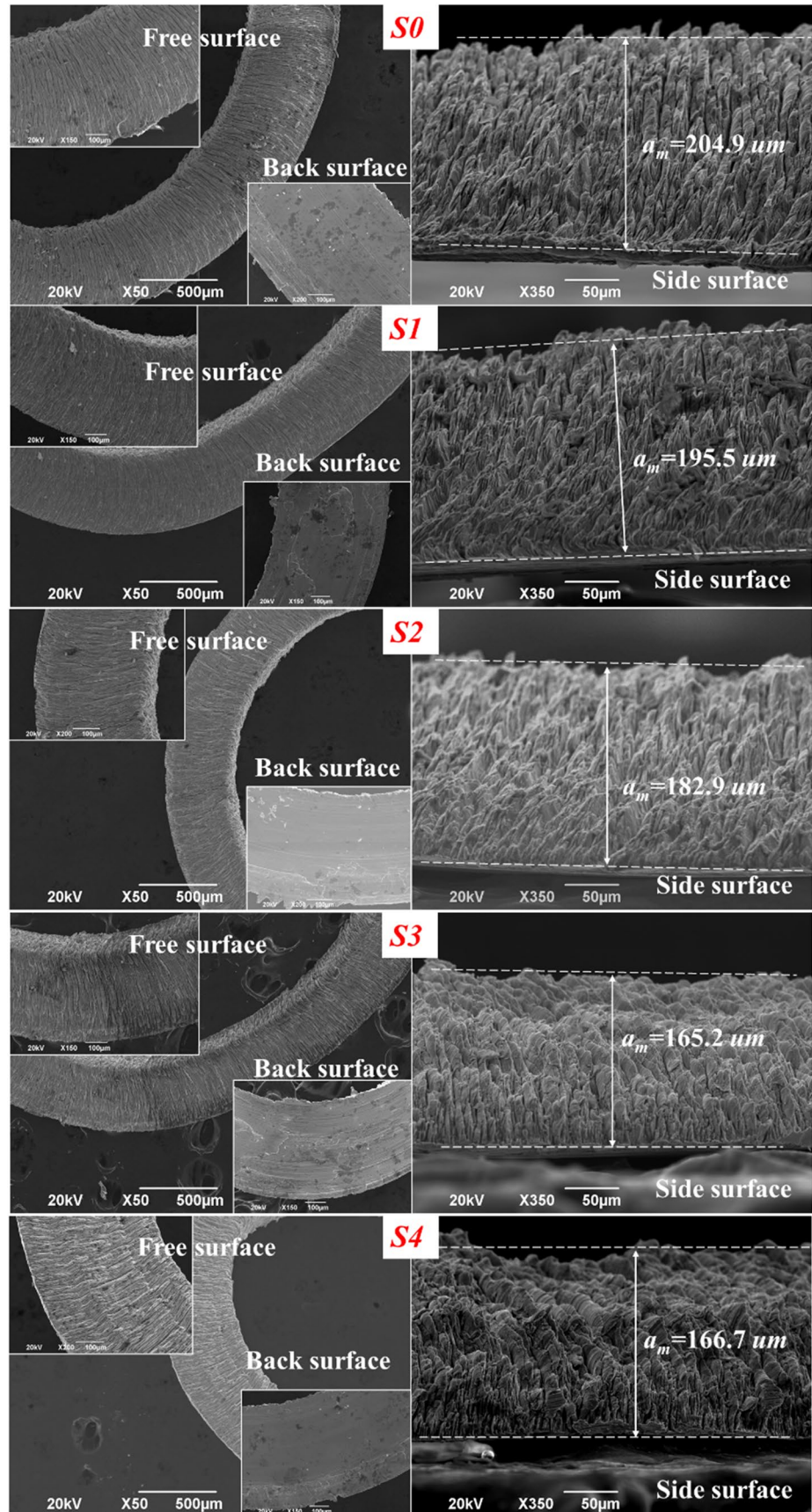


Fig. 8 Equivalent average friction coefficient of cutting tools

Fig. 9 The morphology of chip free surface, back surface, and side surface



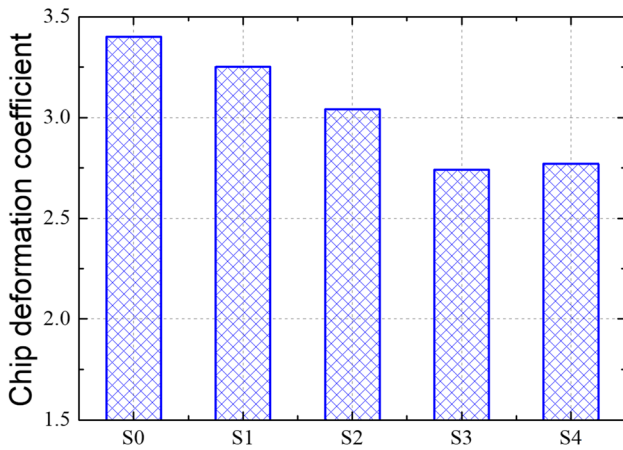


Fig. 10 Chip deformation coefficient of textured and untextured tools

Combining equations (8) and (9), the friction angle decreased gradually with the increase of groove texture width while the shear angle increased, which was consistent with the results calculated based on the measured chip thickness. It can be concluded that the shear angle variation was mainly influenced by the friction characteristics of tool–chip interface. In addition to the chip deformation coefficient, the shear angle can also be used to present the degree of chip shear deformation. The chip shear deformation degree decreased with the increase of shear angle. Therefore, the introduction of groove texture can change the chip morphology during machining. With the increase of groove texture width, the chip deformation degree can be reduced, which was mainly caused by the improvement of friction characteristics at tool–chip interface.

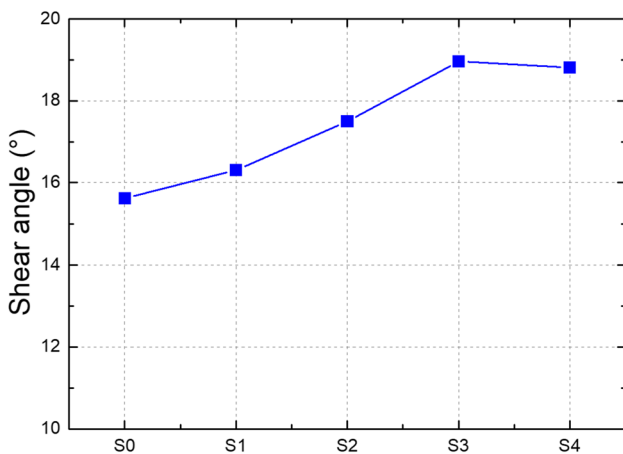


Fig. 11 Shear angle calculated by chip deformation coefficient

4 Stress field redistribution

The micro-grooved textures on tool rake face can reduce the cutting forces and average friction coefficient, which finally improves the friction characteristics of tool–chip interface. The redistribution of stress field on the tool rake face was the main reason for the improvement of friction characteristics. In order to study the influence of groove textures on the redistribution of stress field, the theoretical model of stress field redistribution on the textured tool rake face was proposed and discussed. According to Zorev’s assumption, the normal stress decreased gradually from the maximum value to zero, which can be expressed as

$$\sigma(x) = \sigma_m \left(1 - \frac{x}{l_f} \right)^\eta \tag{14}$$

Besides, the theoretical model of tool–chip contact length can be calculated by equation (6). With a normal stress field distribution index η of 2.5, the calculated results are shown in Fig. 12. It indicated that the theoretical tool–chip contact length decreased from 506 to 429 μm with the increase of groove texture width. In this work, the tool–chip contact zone was analyzed by EDS method. To analyze the tool–chip contact length, the distribution of Fe element on the tool rake face was presented in Fig. 13. Different from the calculated result, the EDS results showed that the tool–chip contact length was almost keep constant with the introduction of groove texture. Here, the change of stress field distribution of textured tools cannot be reflected by Zorev’s assumption. According to Zorev’s assumption, the variation of groove texture does not change the type of normal stress field distribution. The improvement of friction behavior and reduction of cutting force were presented with the decrease of tool–chip contact length. The calculated result of tool–chip contact length was therefore different from that of measured

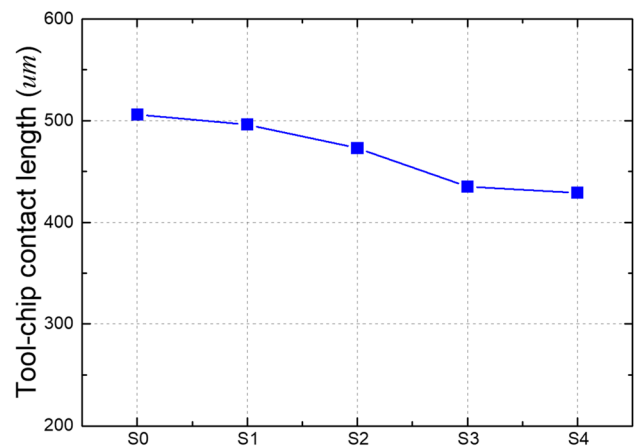
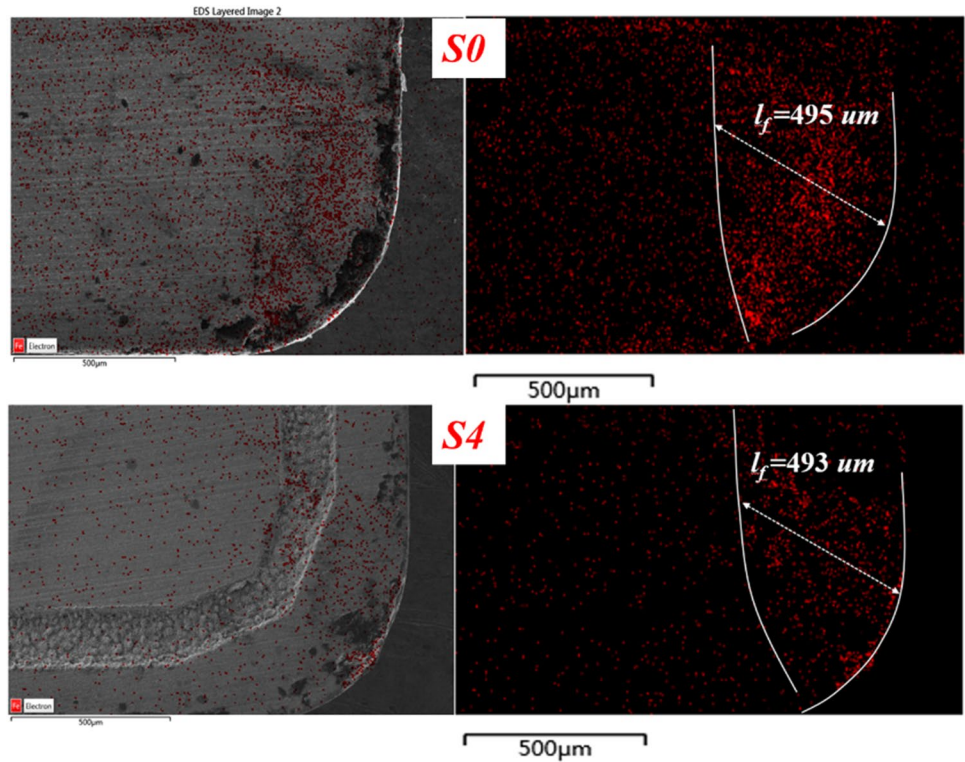


Fig. 12 Theoretical tool–chip contact length

Fig. 13 Distribution of Fe element on the tool rake face



results. Thus, further discussion on the stress field redistribution of textured tools was conducted.

Since the micro-texture and derivative cutting are not considered in Zorev’s assumption, a new stress field distribution model of textured tool was proposed and discussed based on Zorev’s assumption. Several assumptions were made before establishing the stress field redistribution model of micro-groove textured tool. During machining, the cutting fluid in the groove texture mainly played the role of lubrication. The normal stress and shear stress on the cutting fluid in the groove texture zone was much less than those on other locations of tool–chip interface. The stress field at this place was neglected. In order to study the effect of micro-groove texture on stress field distribution, the total tool–chip contact length and maximum normal stress of textured tools were also assumed to be the same as those of untextured tools. Based on above, the normal stress field redistribution on the rake face can be expressed as

$$\sigma(x) = \begin{cases} \sigma_m \left(1 - \frac{x}{l_f}\right)^{\eta_2} & 0 \leq x \leq G_s \\ 0, & G_s < x \leq G_s + G_w \\ \sigma_{m2} \left(\frac{l_f - x}{l_f - G_s - G_w}\right)^{\eta_3}, & G_s + G_w < x \leq l_f \end{cases} \quad (15)$$

where the normal stress field distribution index η_2 was 3 and the maximum normal stress can be calculated by the expression:

$$\sigma_m = F_N \cdot (1 + \eta) / a_w \cdot l_f \quad (16)$$

The derivative cutting on the edge of groove texture can cause the increase of local stress field and generate the derivative maximum normal stress. The derivative maximum normal stress, σ_{m2} , can be expressed as

$$\sigma_{m2} = k \cdot \sigma_m \cdot \left(1 - \frac{G_s + G_w}{l_f}\right)^{\eta_2} \quad (17)$$

Based on above assumptions, the normal stress field distribution of textured tool was different from that of untextured tool in the groove texture and derivative cutting zone, as shown in Fig. 14. The derivative normal stress field distribution index $\eta_3 = 0.2\eta_2$, and the increase factor k was 6. With this model, the normal force variation can be presented clearly. The appearance of groove texture zone will decrease the local normal stress, as shown in Fig. 14. Owing to the derivative cutting, the local normal stress on the edge of groove texture will increase. Then, the normal force variation was mainly caused by the combined influence of them. In order to verify the accuracy of the model, the normal force was calculated. Based on the theoretical model, the normal force of textured tools was calculated by integrating the normal stress, as given by the equation:

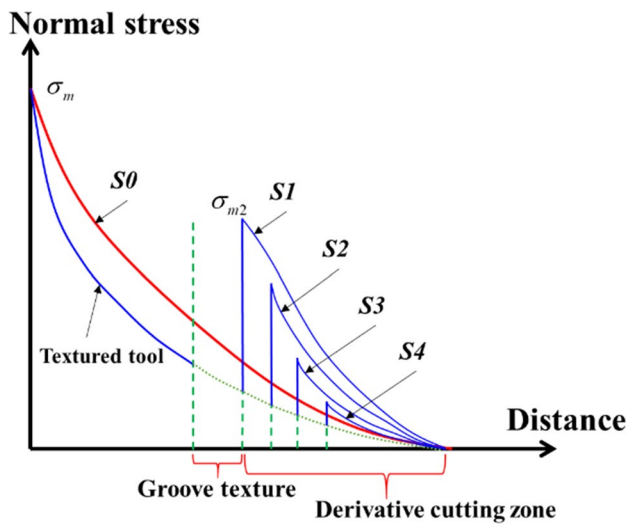


Fig. 14 The normal stress field distribution of textured tools

$$F_N = \int_0^{G_s} a_w \cdot \sigma_m \left(1 - \frac{x}{l_f}\right)^{\eta_2} dx + \sigma_{m2} \cdot \frac{a_w \cdot (l_f - G_s - G_w)}{1 + \eta_3} \tag{18}$$

In addition to the theoretical calculation, the normal force on the textured tool rake face can also be expressed by the measured results of axial force F_x , radial force F_y , and main cutting force F_z as

$$F_N = \sqrt{F_y^2 + F_z^2} \cdot \cos \beta \tag{19}$$

The calculated result of normal force was then compared with the measured result, as shown in Fig. 15. The errors between the calculated and measured results were less than 5%. The results can also verify the reliability of

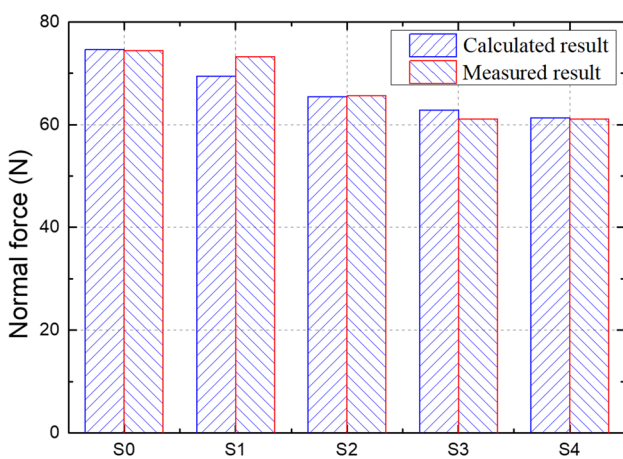


Fig. 15 The calculated and measured results of the normal force of textured and untextured tools

the theoretical model. According to the proposed model, the normal force F_N decreased gradually with the increase of groove texture width G_w . With the increase of groove texture width, the decrease of local normal stress, caused by the groove texture, will be enlarged. And the increase of local normal stress, caused by the derivative cutting, will be reduced. Finally, the normal force decreased with the increase of texture width, as shown in Fig. 15.

In addition, the shear stress redistribution of textured tool at the tool–chip interface can also be expressed as

$$\tau(x) = \begin{cases} \tau_0, & 0 < x \leq l_m \\ u_n \cdot \sigma_m \left(1 - \frac{x}{l_f}\right)^{\eta_2}, & l_m < x \leq G_s \\ 0, & G_s < x \leq G_s + G_w \\ u_n \cdot \sigma_{m2} \left(\frac{l_f - x}{l_f - G_s - G_w}\right)^{\eta_3}, & G_s + G_w < x \leq l_f \end{cases} \tag{20}$$

where τ_0 was the shear yield strength at the tool–chip interface, l_m was the sticking length, and u_n was the sliding friction coefficient. The sticking length l_m can be calculated as

$$l_m = l_f \left[1 - \left(\frac{\tau_0}{u_n \sigma_m}\right)^{1/\eta} \right] \tag{21}$$

Finally, the shear stress field redistribution of textured tool can be presented as shown in Fig. 16.

Based on the theoretical model, the friction force of textured tools can be calculated by

$$F_f = \int_0^{l_m} \tau_0 \cdot a_w dx + \int_{l_m}^{G_s} u_n \cdot \sigma_m \left(1 - \frac{x}{l_f}\right)^{\eta_2} dx + \int_{G_s+G_w}^{l_f} u_n \cdot \sigma_{m2} \left(\frac{l_f - x}{l_f - G_s - G_w}\right)^{\eta_3} dx \tag{22}$$

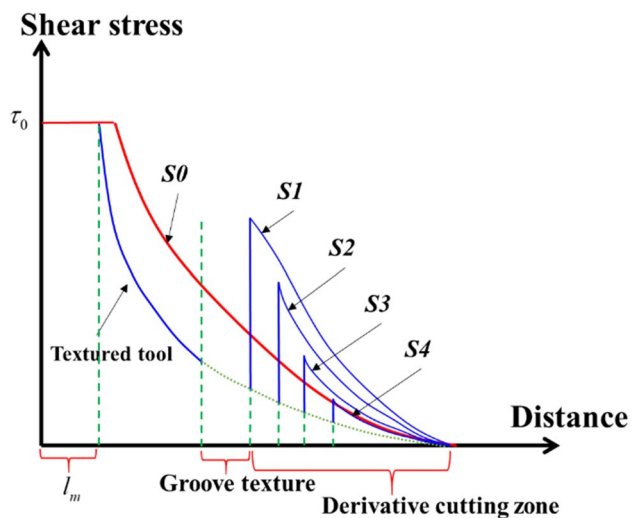


Fig. 16 The shear stress field distribution of textured tools

In addition to the theoretical calculation, the friction force can also be expressed by the measured results as

$$F_f = F_N \cdot \tan\beta \quad (23)$$

The calculated result of friction force was compared with measured result, as shown in Fig. 17. The error between the calculated and measured results was less than 6.5%.

The variation of friction characteristics at the tool–chip interface can then be explained by the stress field redistribution clearly. With the appearance of groove texture, the normal stress and shear stress in the textured zone was almost reduced to zero, and the friction behavior at the tool–chip interface will also be improved. However, derivative cutting will enlarge the local stress field and worsen the friction behavior. Under the combined effect of groove texture and derivative cutting, the equivalent average friction coefficient of textured tools will be improved. The chip deformation degree will also be reduced with the improvement of friction behavior. Thus, the improved theoretical model, proposed in this research based on Zorev's assumption, can effectively describe the stress field redistribution at the tool–chip interface, and explain the variation of normal force, friction force, and friction characteristics.

Micro-textures have been applied in the field of material processing for decades and also showed great potential in the machining of new materials [36]. The present findings have shown that the friction characteristics of the tool–chip interface can be improved with the introduction of micro-textures. The chip deformation degree can also be influenced by groove textures. Based on Zorev's assumption, improved theoretical model of stress field redistribution was proposed, which can present the friction characteristics variation on the rake face more clearly. The textured area reduced the local stress and improved the friction behavior, which also generated derivative cutting and enlarged local stress. Then, the variation of normal force, friction force, and friction

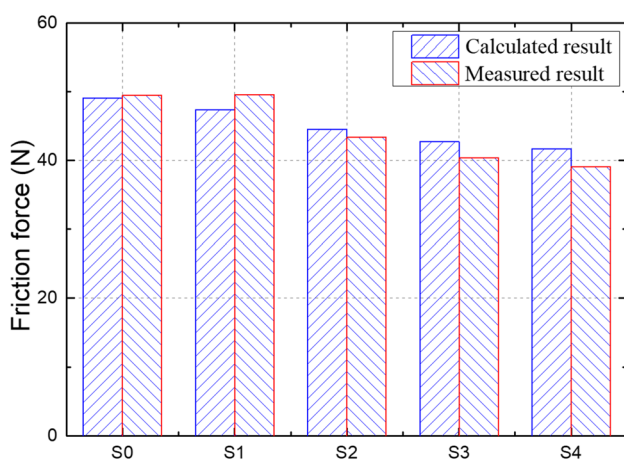


Fig. 17 The calculated result and measured result of friction force

characteristics was mainly determined by the combined effect of them. The present findings provide a new approach to reveal the friction mechanism of micro-textured tools at the tool–chip interface.

5 Conclusions

The effect of micro-textures on the cutting performance and friction behavior at tool–chip interface was studied comprehensively in terms of cutting force, friction characteristics, chip deformation, and stress field redistribution. The main findings are concluded as follows:

- (1) Groove textures can reduce the main cutting forces by 18% with the reducing of average shear strength and tool–chip contact area. On the other hand, derivative cutting will come up at the edge of groove texture, which can cut the bottom of the chip, and enlarge the local stress. With the increase of groove texture width G_w , the reduction of cutting force will be enlarged, and the effect of derivative cutting reduced.
- (2) The equivalent average friction coefficient on the tool–chip interface was calculated with considering of axial force F_x . The equivalent average friction coefficient u_a , which can usually be used to characterize the friction characteristics, decreases gradually with the increase of groove texture width G_w . The introduction of groove texture can also change the chip deformation coefficient and reduce the chip deformation degree, which was mainly caused by the improvement of friction characteristics at the tool–chip interface.
- (3) Based on Zorev's assumption, an improved theoretical model of stress field redistribution for micro-textured tool was proposed. The model can be used to calculate the normal force F_N and friction force F_f . With the increase of groove texture width, the decrease of normal and shear stress in the groove texture zone will be enlarged, and the increase of normal and shear stress, caused by the derivative cutting, will be reduced. Under the combined effect of groove texture and derivative cutting, the friction characteristics at the tool–chip interface will be improved, and its variation rule can be presented more clearly.

Author contribution Junsheng Zhang: review, conceptualization, methodology, validation, writing original draft, and writing—review. Yongsen Shang: material preparation and data collection. Haidong Yang: conceptualization, methodology, and validation. Huohong Tang: writing—review and editing. Shunhua Chen: conceptualization and writing—review and editing.

Funding This work was mainly supported by the Natural Science Foundation of Anhui Province (grant number 2108085ME171), Key Laboratory of Electric Drive and Control of Anhui Province (grant number DQKJ202101), and Fundamental Research Funds for the Central Universities (grant number JZ2022HGTB0247).

Data availability The raw/processed data will be made available on request.

Code availability This is not applicable.

Declarations

Ethics approval This is not applicable.

Consent to participate This is not applicable.

Consent for publication This is not applicable.

Conflicts of interest The authors declare no competing interests.

References

- Zhang G, Chen B, Wu G, Xie G, Xie H (2022) Experimental assessment of textured tools with nano-lubricants in orthogonal cutting of titanium alloy. *J Mech Sci Technol* 36(5):2489–2497
- Liu X, Liu Y, Li L, Tian Y (2019) Performances of micro-textured WC-10Ni3Al cemented carbides cutting tool in turning of Ti6Al4V. *Int J Refrac Metals Hard Mat* 84:104987
- Gupta MK, Song QH, Liu ZQ, Singh R, Sarikaya M, Khanna N (2021) Tribological behavior of textured tools in sustainable turning of nickel based super alloy. *Tribol Int* 155:106775
- Alagan NT, Zeman P, Hoier P, Beno T, Klement U (2019) Investigation of micro-textured cutting tools used for face turning of alloy 718 with high-pressure cooling. *J Manufact Proc* 37:606–616
- Sharma V, Pandey PM (2016) Recent advances in turning with textured cutting tools: a review. *J Clean Prod* 137:701–715
- Arslan A, Masjuki HH, Kalam MA, Varman M, Mufti RA, Mosarof MH, Khuong LS, Quazi MM (2016) Surface texture manufacturing techniques and tribological effect of surface texturing on cutting tool performance: a review. *Cr Rev Solid State Mater Sci* 41:447–481
- Orra K, Choudhury SK (2018) Tribological aspects of various geometrically shaped micro-textures on cutting insert to improve tool life in hard turning process. *J Manufact Proc* 31:502–513
- Kümmel J, Braun D, Gibmeier J, Schneider J, Greiner C, Schulze V, Wanner A (2015) Study on micro texturing of uncoated cemented carbide cutting tools for wear improvement and built-up edge stabilization. *J Mater Process Technol* 215:62–70
- Sugihara T, Enomoto T (2017) Performance of cutting tools with dimple textured surfaces: A comparative study of different texture patterns. *Precis Eng* 49:52–60
- Gajrani KK, Suresh S, Sankar MR (2018) Environmental friendly hard machining performance of uncoated and MoS₂ coated mechanical micro-textured tungsten carbide cutting tools. *Tribol Int* 125:141–155
- Lu P, Wood RJK (2020) Tribological performance of surface texturing in mechanical applications—a review. *Surf Topogr: Metrol Prop* 8:043001
- Sangjin M, Hiroaki I, Yasuhiro K, Sangkee M (2022) Study on cutting force and tool wear in machining of die materials with textured PCD tools under ultrasonic elliptical vibration. *Int J Precis Eng Manuf-Green Technol* 10:35–44
- Sugihara T, Kobayashi R, Enomoto T (2021) Direct observations of tribological behavior in cutting with textured cutting tools. *Int J Mach Tools Manuf* 168:103726
- Chen YH, Wang J, An QL (2021) Mechanisms and predictive force models for machining with rake face textured cutting tools under orthogonal cutting conditions. *Int J Mech Sci* 195:106246
- Orra K, Choudhury SK (2021) Experimental investigation of machining process by micro-textured cutting insert together with magneto-rheological damper. *Wear* 476:203731
- Siju AS, Waigaonkar SD (2021) Effects of rake surface texture geometries on the performance of single-point cutting tools in hard turning of titanium alloy. *J Manuf Proc* 69:235–252
- Sun XY, Wang XY, Hu YW, Duan JA (2021) The effect of micro-texture on wear resistance of WC/Co-based tools during cutting Ti-6Al-4V. *App Physics A* 127:453
- Kishawy HA, Salem A, Hegab H, Hosseini A, Balazinski M (2021) Micro-textured cutting tools: Phenomenological analysis and design recommendations. *CIRP Annals-Manuf Technol* 70:65–68
- Zou ZF, He L, Jiang HW, Yuan S, Ren ZW (2021) Influence of microgroove structure on cutting performance and chip morphology during the turning of superalloy Inconel 718. *Materials* 14:4142
- Hou QM, Yang XF, Li D, Cheng J, Wang SR, Xiao JP, Li WY (2022) Tribological performance of hydrophobic and micro/nano triangle textured rake face of cutting tools. *App Surface Sci* 571:151250
- Amal SS, Sandeep J, Sachin DW (2022) Experimental analysis and characterisation of chip segmentation in dry machining of Ti-6Al-4V alloy using inserts with hybrid textures. *CIRP J Manuf Sci Technol* 36:213–226
- Fouathiyah A, Meziani S, Sahli M, Barriere T (2021) Experimental investigation of microtextured cutting tool performance in titanium alloy via turning. *J Manuf Proc* 69:33–46
- Zhou Y, Fu YH, Yang J (2022) Effect of volcano-like textured coated tools on machining of Ti6Al4V: an experimental and simulative investigation. *Int J Adv Manuf Technol* 120:7785–7802
- Avadhoot R, Satish C (2022) Experimental investigation on laser-processed micro-dimple and micro-channel textured tools during turning of Inconel 718 alloy. *J Mater Eng Perform* 31:4068–4083
- Takahashi W, Nakanomiya T, Suzuki N, Shamoto E (2021) Influence of flank texture patterns on the suppression of chatter vibration and flank adhesion in turning operations. *Precis Eng* 68:262–272
- Wang QW, Yang Y, Yao P, Zhang ZY, Yu SM, Zhu HT, Huang CZ (2021) Friction and cutting characteristics of micro-textured diamond tools fabricated with femtosecond laser. *Tribol Int* 154:106720
- Duan R, Wang GJ, Xing YQ (2022) Investigation of novel multi-scale textures for the enhancement of the cutting performance of Al₂O₃/TiC ceramic cutting tools. *Ceramics Int* 48:3554–3563
- Siju AS, Gajrani KK, Joshi SS (2021) Dual textured carbide tools for dry machining of titanium alloys. *Int J Refrac Metals Hard Mat* 94:105403
- Mishra SK, Ghosh S, Aravindan S (2020) Machining performance evaluation of Ti6Al4V alloy with laser textured tools under MQL and nano-MQL environments. *J Manuf Proc* 53:174–189
- Gajrani KK, Suvin PS, Kailas SV, Rajurkar KP, Sankar MR (2021) Machining of hard materials using textured tool with minimum quantity nano-green cutting fluid. *CIRP J Manuf Sci Technol* 35:410–421

31. Zhang YP, Guo XH, Li ZH, Wang CD, Liu TS, Zhang KD (2022) Study on the tribological properties of Fe_3O_4 @CNTs nanofluids acting on the textured ceramics. *App Physics A* 128:161
32. Zhang L, Guo XH, Zhang KD, Wu YQ, Huang Q (2020) Enhancing cutting performance of uncoated cemented carbide tools by joint use of magnetic nanofluids and micro-texture under magnetic field. *J Mater Proc Technol* 284:116764
33. Guo XH, Huang Q, Wang CD, Liu TS, Zhang YP, He HD, Zhang KD (2022) Effect of magnetic field on cutting performance of micro-textured tools under Fe_3O_4 nanofluid lubrication condition. *J Mater Proc Technol* 299:117382
34. Zhang JS, Yang HD, Chen SH, Tang HH (2020) Study on the influence of micro-textures on wear mechanism of cemented carbide tools. *Int J Adv Manuf Technol* 108:1701–1712
35. Xing YQ, Deng JX, Wu Z, Liu L, Huang P, Jiao A (2018) Analysis of tool-chip interface characteristics of self-lubricating tools with nanotextures and WS_2/Zr coatings in dry cutting. *Int J Adv Manuf Technol* 97:1637–1647
36. Chen SH, Ge Q, Zhang JS, Chang WJ, Zhang JC, Tang HH, Yang HD (2021) Low-speed machining of a Zr-based bulk metallic glass. *J Manuf Proc* 72:565–581

Publisher's note Springer Nature remains neutral with regard to jurisdictional claims in published maps and institutional affiliations.

Springer Nature or its licensor (e.g. a society or other partner) holds exclusive rights to this article under a publishing agreement with the author(s) or other rightsholder(s); author self-archiving of the accepted manuscript version of this article is solely governed by the terms of such publishing agreement and applicable law.